CHEMISTRY
A EUROPEAN JOURNAL

DOI: 10.1002/chem.200800906

Reaction Mechanism of Molybdoenzyme Formate Dehydrogenase

Monica Leopoldini, Sandro G. Chiodo, Marirosa Toscano, and Nino Russo*[a]

Abstract: Formate dehydrogenase is a molybdoenzyme of the anaerobic formate hydrogen lyase complex of the *Escherichia coli* microrganism that catalyzes the oxidation of formate to carbon dioxide. The two proposed mechanisms of reaction, which differ in the occurrence of a direct coordination or not of a SeCys residue to the molybdenum metal during catalysis were analyzed at the density functional level in both vacuum and protein environments. Some DF functionals, in addition to the very popular B3LYP one, were employed to compute barrier heights. Results revealed the role played by the SeCys residue in performing the abstraction of the proton from the formate substrate. The computation of the energetic profiles for both mechanisms indicated that the reaction barriers are higher when the selenium is directly coordinated to the metal, whereas less energy is required when SeCys is not a ligand at the molybdenum site.

Keywords: catalysis · density functional calculations · enzymes · oxidation · selenocysteine

Introduction

Molybdenum is a widespread metal in biological systems and it is mainly contained in two classes of enzymes: the nitrogen-fixating nitrogenases, which have an iron–molybdenum cofactor,[1] and the mononuclear molybdenum enzymes (molybdoenzymes).[2] The latter catalyze oxygen-atom transfer reactions to and from biological substrates in the nitrogen, sulfur and carbon cycles.[3]

On the basis of the coordination at the active site, the molybdoenzymes are subdivided into three families: the xanthine oxidase, the sulfite oxidase and the dimethysulfoxide (DMSO) reductase.[2,4] All of them possess an organic pterin cofactor that contains a dithiolene moiety, the molybdopterin guanine dinucleotide (MGD). The cofactor is usually found to be coordinated by the dithiolene sulfur atoms to the metal.[5]

Formate dehydrogenase, FDH (EC: 1.2.1.2), belongs to the DMSO reductase family and catalyzes the oxidation of formate to carbon dioxide. The enzyme from anaerobic bacteria is bound to membranes and is typically found to possess molybdenum, whereas the enzyme from archaea may contain either a molybdenum or tungsten centre.[2] Even if it is a member of the DMSO reductase family, FDH does not catalyze oxygen-atom transfer reactions, but favours the cleavage of a C–H bond.[2] FDH contains a selenocysteine residue bound to the Mo centre which is crucial for its catalytic activity.

In *E. coli*, three FDHs are expressed, namely FDH-N, FDH-O and FDH-H. FDH-H is a part of the formate–hydrogen lyase complex of *E. coli* that is expressed under anaerobic conditions, and it is involved in biological hydrogen production from formate through fermentative processes.[6–8]

The first crystal structure of both oxidized and reduced FDH-H was solved by Boyington et al.[8] The structure is made up by four α/β domains, and among them domain I coordinates a Fe_4S_4 cluster, which is involved in the electron flow. Domains II and III bind the two MGD cofactors. The molybdenum, which is coordinated to two cofactors, the Fe_4S_4 cluster and the selenocysteine residue, are central to the catalytic activity.

In the reduced Mo^{IV} form, the molybdenum in the active site is coordinated by four sulfur atoms, which come from the cofactors, and by the selenium atom of the SeCys140 residue. Other residues, His141 and Arg333, are well conserved in all Mo-containing formate dehydrogenases.

[a] Dr. M. Leopoldini, Dr. S. G. Chiodo, Prof. Dr. M. Toscano, Prof. Dr. N. Russo
Dipartimento di Chimica and Centro di Calcolo ad Alte Prestazioni per Elaborazioni Parallele e Distribuite-Centro d'Eccellenza MIUR, Universita' della Calabria
I-87030 Arcavacata di Rende (CS) (Italy)
Fax:
E-mail: nrusso@unical.it

Supporting information for this article is available on the WWW under http://dx.doi.org/10.1002/chem.200800906.

The oxidized Mo^{VI} form, in complex with the nitrite inhibitor, shows a Mo–O bond length of 2.58 Å; the other oxygen atom is involved in a hydrogen bond with the positive Arg333 residue.[8]

On the basis of the crystallographic data concerning both the oxidized and the reduced form of the enzyme, Boyington et al. proposed a reaction mechanism, which is reported in Scheme 1 (mechanism A).[8] The catalysis starts with the coordination of the formate substrate by its oxygen atom to the molybdenum, probably by replacing a SH ligand. Weak interactions are established between the formate and the nearby residues His141 and Arg333. The selenium atom abstracts the proton by cleaving the C–H bond in the substrate, while two electrons are transferred to the Mo centre. Upon oxidation, the proton is most likely transferred from the selenocysteine to the His141 residue. The Mo^{VI} form is restored in another step, with the two electrons travelling to the Fe_4S_4 cluster through the MGD moiety.

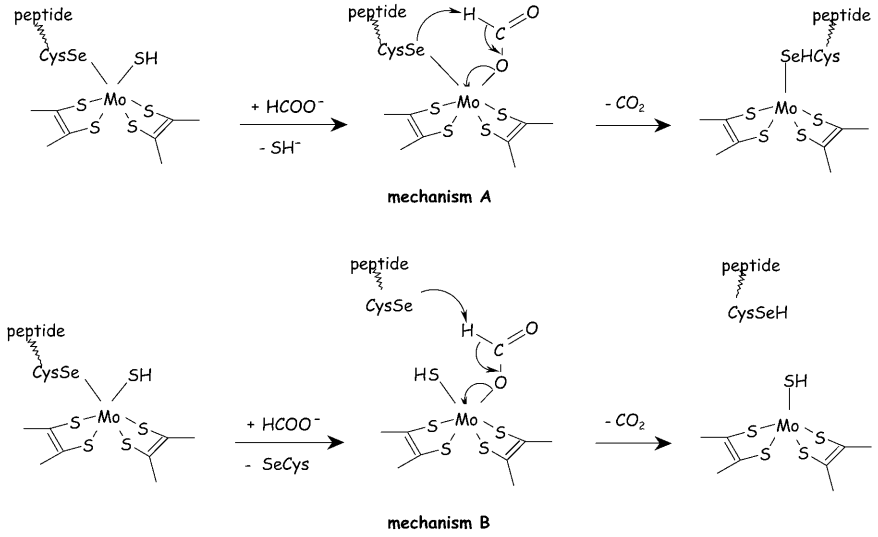

Scheme 1. Bound SeCys (A) and unbound SeCys (B) reaction mechanisms proposed for the oxidation of formate to carbon dioxide by FDH.

Recently, another formate-reduced *E. coli* FDH crystal structure was solved by Raaijmakers et al. at 2.27 Å.[9] In this structure, the selenium atom of the SeCys140 residue is located 12 Å away from the molybdenum; this implies that the selenium is not a metal ligand in the reduced form of the enzyme. Furthermore, Arg333 with its positive charge establishes a salt-type interaction with the negative selenol group. A SH group (or S^{2-}) is identified as the apical ligand at the Mo centre rather than a hydroxyl/water ligand. By taking into account these latter experimental data, Raaijmakers et al. proposed a new mechanism for the formate oxidation; this is schematically depicted in the Scheme 1 and referred to as mechanism B.[9] The formate binding displaces the selenocysteine ligand, which, once away from the metallic centre, interacts through a hydrogen bond with the Arg333 residue. The SH group is retained as the Mo ligand. Also in this mechanism, the negative selenol abstracts the proton from the substrate to give the CO_2 product, which is released from the active site, and to the Mo^{IV} form of the enzyme. The latter mechanism seems to be supported by EPR studies on *Desulfovibrio desulfuricans* FDH according to which SH is retained in the Mo^{V} state of the enzyme upon CO_2 formation.[10]

The two mechanisms, A and B, differ in the role played by the SeCys140 residue as a Mo ligand or in an unbound form during catalysis.[8,9]

With the aim of determining which mechanism represents the preferred reaction path that is followed by FDH enzyme, we performed a density-functional-based study on formate oxidation by using a Mo-containing cluster as simplified model of the active site.

Method

All the computations were carried out with the Gaussian 03 code, Revision C.02.[11] The hybrid Becke exchange and Lee, Yang and Parr correlation (B3LYP) functional was used to perform geometry optimization.[12–15] The 6–31+G* basis set was chosen for the C, N, O, S, Se and H atoms,[16–19] whereas the LANL2DZ pseudo-potential in connection with the relative orbital basis set[20] was used for the metal.

Frequency calculations were performed on all stationary points of the reaction paths to evaluate their character as minima or saddle points, and to compute zero-point energy corrections, which were then included in all the relative energy values.

Intrinsic reaction coordinate (IRC) calculations[21,22] were performed with the aim to confirm that a given transition state connects a particular couple of consecutive minima.

The check of stability for the open-shell optimised structure wave functions was carried out by means of the Stable procedure implemented in the G03 code.[23–25]

Solvent effects were introduced as single-point computations on the optimised gas-phase structures in the framework of Self Consistent Reaction Field Polarisable Continuum Model (SCRF-PCM),[26–28] in which the cavity is created by a series of overlapping spheres. The United Atom Topological (UAO) Model applied on atomic radii of the UFF force field[29] was used to build the cavity in the gas-phase equilibrium geometry. The dielectric constant value $\varepsilon = 4$ was chosen by taking into account the coupled effect of the protein itself and the water medium that surrounds the protein, according to previous suggestions.[30–36] The relative solvent effects between minima and transition states are normally calculated to be quite small, within 2 kcal mol^{-1}.[30,31]

The performance of the B3LYP functional in predicting properties of transition-metal-containing systems is well supported by the literature, especially concerning enzymatic catalysis.[30–36] It still represents the most widely used DF functional. However, new functionals were developed during the last decade and tested towards several chemical properties, including the determination of barrier heights.[37] For the B3LYP, a tendency to underestimate this quantity was observed in some cases,[38–42] even if it is a valid method for some chemical properties, such as geometry determination and calculation of atomisation energies and other thermochemical quantities.[37] Recently, BB1K[43] and MPWB1K[44] have been proposed as effective tools for the calculation of barrier heights, thermochemical kinetics and non-bonded interactions. Taking into account these studies and the growing use of DFT methods for enzymatic catalysis, it is important to investigate the suitability of alternative functionals for studying enzymatic reactions. So, for the purpose of comparison, we have employed different exchange–correlation functionals to compute barrier heights. In addition to B3LYP, the BHandHLYP[12,13,15] and the PBE1PBE,[45] as examples of hybrid generalized gradient approximation (H-GGA) functionals, were considered. The MPWB1K[44,46,47] and BB1K,[15,43,46] which belong to the class of hybrid-meta GGA (HM-GGA) methods were also chosen.

The active-site model cluster that was used in this work was built by starting from the 2.9 Å X-ray structure of the oxidized form of formate dehydrogenase H from *E. coli*, which was complexed with the inhibitor nitrite (PDB code = 1FDI).[8] The cluster is made up of a Mo–bis(dithiolene) complex that reproduces the $[Mo(mgd)_2]$ complex, by the dipeptide SeCys140-His141, by the $CH_3CH_2NHC(NH_2)_2^+$ group, modelling the Arg333 residue, and an SH^- (see Scheme 2). Similar cluster models were successfully used to theoretically mimic the active site of molybdoenzymes.

An atom of each amino acid residue and of the MGD models was kept frozen at its crystallographic position to mimic the steric effects produced by the surrounding protein, and to avoid an unrealistic expansion of the cluster during the optimization procedure. The substrate $HCOO^-$ and the product CO_2 were left free from constraints during the optimization procedure.

Natural bond orbital (NBO) analysis[48] was carried out to determine net charges and some electronic properties.

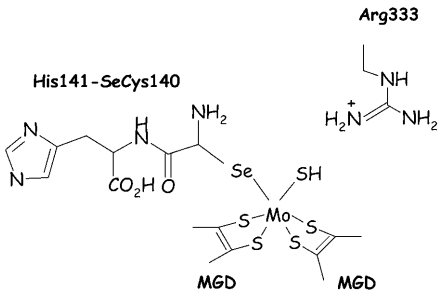

Scheme 2. Model used for the FDH active site.

Results and Discussion

Mechanism A: To our knowledge, no experimental data exist on the electronic ground state of molybdoenzymes active site. Experimental studies on molybdoenzymes suggested a diamagnetic state for both Mo^{IV} and Mo^{VI}.[49] In a photoelectron spectroscopy study on the $[Mo^{IV}O(mnt)_2]^{2-}$ (mnt = maleonitriledithiolate) complex, the singlet configuration was indicated to be the ground state, even if no further electronic states were taken into account.[50] Because the multiplicity of the species involved in the catalytic cycle is far from certain, we have explored both the singlet and triplet potential energy surfaces (PES), as encountered for the DF/B3LYP computations on the nitrate reductase enzyme.[33]

The minimized structures of all the stationary points that belong to the reaction catalytic sequence of Scheme 1 for mechanism A are sketched in Figure 1, for singlet (Figure 1a) and triplet (Figure 1b) multiplicities, respectively.

The complex between the $HCOO^-$ substrate and the enzyme, ESa, is obtained when the former coordinates the Mo at 2.05 Å, for both the singlet and triplet. The selenium atom, which is bound to molybdenum at 2.55 (singlet) and

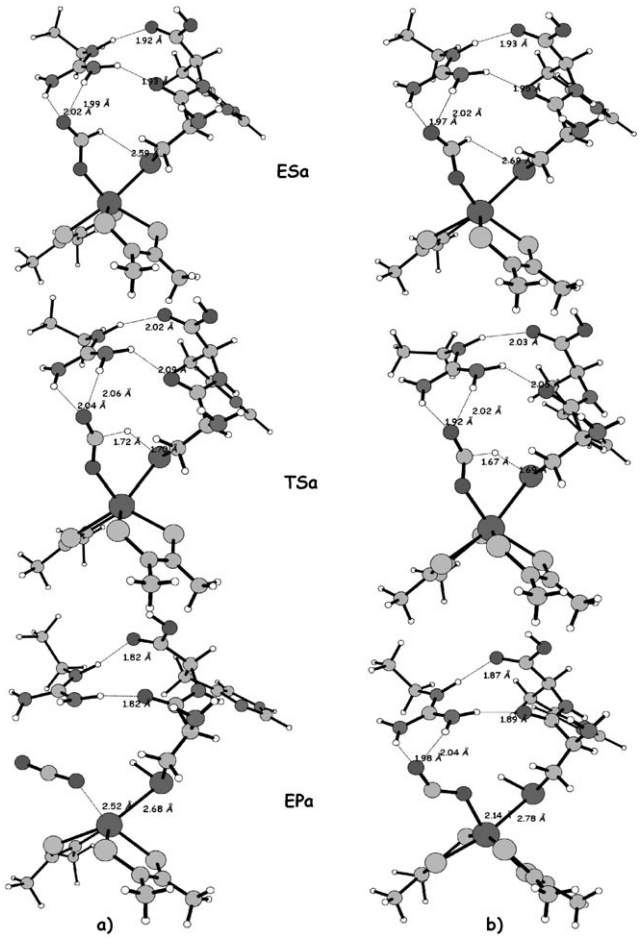

Figure 1. B3LYP-optimised geometries for the stationary points that belong to mechanism A, for singlet (a) and triplet (b) states, respectively.

at 2.61 Å (triplet) lies in a good position to perform the H abstraction from the formate (Se–H distance is 2.59 and 2.69 Å for the singlet and triplet, respectively). This adduct is stabilized by some hydrogen bonds between the Arg333 and the formate, and the Arg333 and the carbonyl oxygen atoms from the SeCys-His dipeptide (see Figure 1).

The reaction passes through a transition state, TSa, that is characterised by the C–H and H–Se critical distances of 1.72 and 1.70 Å, for singlet, and 1.67 and 1.69 Å, for triplet. The vibrational normal modes that occur at the imaginary frequencies of 1022 and 1056 cm^{-1} correspond to the stretching of the C–H and H–Se bonds. The same type of weak interactions established in the ESa species are retained in the structures of the transition states (see Figure 1).

Upon oxidation of the substrate to carbon dioxide, the reaction evolves towards the complex between the active site and the product, EPa. As far as the singlet electronic state is concerned, the CO_2 molecule in the EPa species appears to be practically not coordinated to the molybdenum (the O–Mo distance is 2.52 Å) and arranges itself in a linear disposition. As a consequence of the protonation of selenium of selenocysteine, the Mo–Se distance lengthens up to 2.68 Å. Hydrogen bonds are found between the peptide NH and terminal NH_2 groups of Arg333 and the carbonyl oxygen atoms of the SeCys–His dipeptide (see Figure 1).

In the case of the triplet multiplicity, the EPa complex is characterized by an angular CO_2 molecule still bound to the Mo at 2.14 Å, whereas the Se–Mo distance is computed to be 2.78 Å. As a consequence, one oxygen atom from the CO_2 is involved in two H bonds with the Arg333 NH_2 groups (1.98 and 2.04 Å). So, the product molecule is not released from the metallic site when the enzyme is in the triplet electronic state.

All structures of the stationary points for both singlet and triplet, are well described as trigonal prisms. The only exception is represented by the EPa complex in the triplet electronic state, the structure of which is closer to the octahedral geometry (see Figure 1b). This is due to the fact that, in this multiplicity, the CO_2 is a good π-donor ligand, as its angular disposition may confirm. In the other stationary points, σ bonding involving the d orbitals of molybdenum seems to favour the trigonal prismatic arrangement. This preference for the trigonal prismatic rather than for the octahedral coordination around the metal as a function of the σ and π-donor character of the ligands was already described elsewhere.[33,51]

Mechanism B: The B3LYP-optimized geometries of the species belonging to the reaction catalytic sequence of Scheme 1 for mechanism B are sketched in Figure 2, for singlet (Figure 2a) and triplet (Figure 2b) multiplicities, respectively.

The singlet ESb species shows a formate molecule bound to the molybdenum atom through the oxygen atom at 2.07 Å, whereas the SH group is located 2.43 Å away from the metallic centre. The negatively charged selenium of the selenocysteine residue is involved in a H bond with the positive NH_2 group of the Arg333 (2.31 Å). As a consequence, the distance between the hydrogen atom of the substrate and the selenium is 5.16 Å. This kind of interaction was also found by Raaijmakers et al. in the reduced Mo^{IV} formate dehydrogenase crystal structure,[9] and is claimed to be a direct indication for the mechanism B.

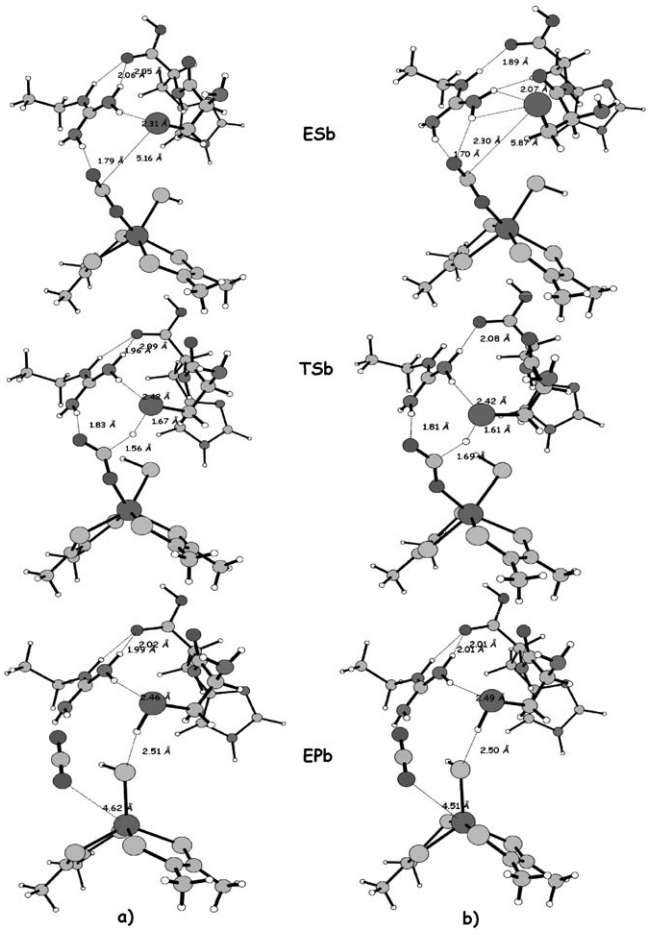

Figure 2. B3LYP-optimised geometries for the stationary points that belong to the mechanism B, for singlet (a) and triplet (b) states, respectively.

Other hydrogen bonds are established between the formate oxygen atom and one of two NH_2 groups, and between the terminal carboxyl of the SeCys–His dipeptide and both the NH and NH_2 moieties of Arg333.

For the ESb in the triplet state, the $O_{formate}$–Mo and the Mo–SH distances are 2.12 and 2.54 Å, respectively. In this species, both the terminal Arg333 NH_2 groups are involved in two H bonds with the formate-unbound oxygen (bond lengths are 1.70 and 2.30 Å, see Figure 2). Because of this, one of the NH_2 groups of the arginine amino acid weakly interacts with both the selenium and peptide carbonyl oxygen atoms, but not with the terminal COOH of the SeCys–His sequence.

The transition states in the two different multiplicities, the nature of the saddle points of which is confirmed by the imaginary frequencies at 907 and 416 cm^{-1}, respectively, are

characterized by the same network of hydrogen bonds that involves the unbound oxygen atom of the substrate and the terminal Arg333 NH_2, and the other Arg333 NH_2 group and both the selenium and the carboxyl oxygen atom (see Figure 2). The C–H and H–Se bonds assume values of 1.56 and 1.67 Å, and 1.69 and 1.61 Å, for the singlet and triplet, respectively.

In the EPb species, the CO_2 molecule is released from the molybdenum centre (O–Mo distance is 4.62 and 4.51 Å, for the singlet and triplet, respectively). The SH group is retained as a Mo ligand, and is involved in a hydrogen bond with the protonated selenium (see distances in Figure 2). Also for this adduct, the selenocysteine and the arginine residues are involved in a weak interaction (NH_2–SeH distance is 2.46 and 2.49 Å, for the singlet and triplet, respectively). The coordination around the molybdenum in the low-spin electronic state is square pyramidal, but for the high-spin state the ligands are arranged in a distorted trigonal bipyramidal geometry. The other stationary points can all be described as trigonal prismatic, as in the case of mechanism A.

The EPb adduct in the low-spin state possesses a structure that is very similar to that shown by the *E. coli* FDH-H reduced form obtained by Raaijmakers et al.[9] The coordination around the Mo atom is best described as a square pyramid in both cases. The average Mo–$S_{dithiolene}$ distance is 2.32 and 2.36 Å, in the crystal and optimised structure, respectively. The apical sulfur atom is located at 2.07 Å in the crystal structure, and at 2.44 Å in the B3LYP one. This discrepancy might be due the fact that the apical ligand in the crystallographic structure could be a S^{2-} ion rather than SH^-, as questioned by authors.

The selenocysteine residue is still in the active site in the EPb-optimised structure (Mo–Se distance is 6.13 Å). This means that it retains a very slight interaction with Arg333. Instead, this residue lies at 12.23 Å from Mo in the crystal structure.[9] However, even if the crystal structure could refer to a later step of the catalytic process, the hydrogen-bonding pattern between the SeCys140 and Arg333 is well reproduced.

Energetics of the two reaction mechanisms: The potential energy surfaces (PESs) for both oxidation mechanisms A and B of the formate substrate by the Mo-containing cluster in the gas phase and in the protein environment (values in parenthesis) are reported in Figure 3.

For both reaction paths, the rate-determining step is the hydrogen abstraction from the carbon atom of the substrate, which is performed by the selenium of the SeCys residue.

As far as mechanism A, which involves the SeCys140 residue as a Mo ligand, is concerned the two ESa complexes in the different multiplicities are practically degenerate (the gas-phase energetic gap is only 0.9 kcal mol^{-1} and it becomes 0.2 kcal mol^{-1} as far as the protein environment is concerned), so they may coexist.

TSa is found at 35.6 (singlet) and 38.6 kcal mol^{-1} (triplet), above the initial minimum. Product complexes lie at 24.0 and 33.9 kcal mol^{-1}, for the singlet and triplet, respectively.

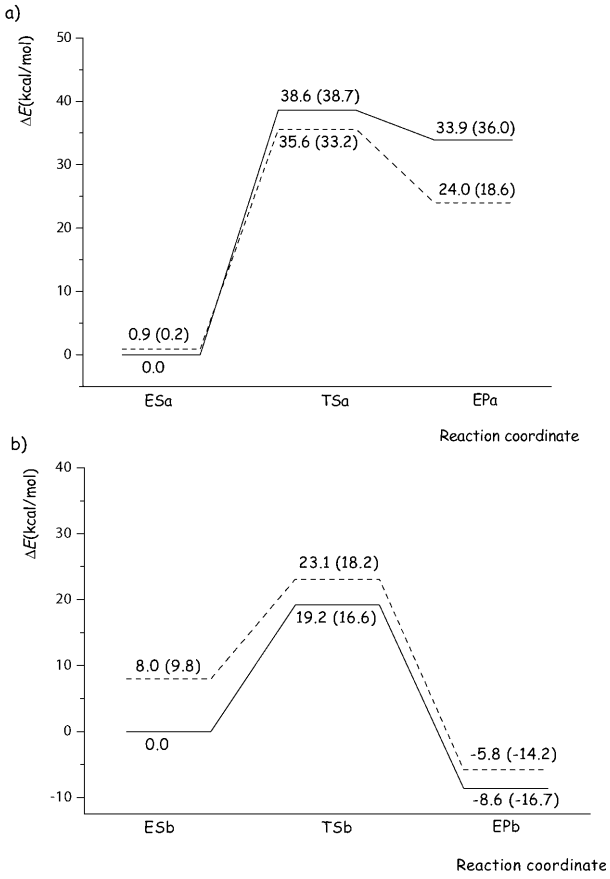

Figure 3. B3LYP potential energy profiles for mechanisms A (a) and B (b), in the gas phase and protein environment (values in parenthesis). -----: singlet state, ——: triplet state ($\varepsilon = 4$)

Although the energetic profile seems to be more favourable for the reaction in the ground state, the activation energies required to oxidize the substrate to carbon dioxide are in both cases very high (34.7 and 38.6 kcal mol^{-1}, for singlet and triplet, respectively). In addition, the complex between the reduced active site and the CO_2, in which the latter is still bound to Mo, is decidedly less stable than ESa, so that the reaction turns out to be very endothermic.

The presence of the protein environment, which is described by a dielectric constant of $\varepsilon = 4$, does not introduce meaningful effects, except for a strong stabilisation of the EPa complex in the singlet state; this, however, does not change the thermodynamic of the process.

In the mechanism in which the SeCys140 is in the unbound form (mechanism B), the energy gap between the singlet and triplet ESb species is 8 kcal mol^{-1}; the triplet is the minimum-energy structure.

Transition states are found at 23.1 and 19.2 kcal mol^{-1}, for the singlet and triplet, respectively.

Finally, products are found 5.8 and 8.6 kcal mol^{-1} below the minimum.

The triplet potential energy profile lies below that obtained for the low-spin state, thus representing the minimum energy path.

As can be immediately noted from the PESs shown in Figure 3, in mechanism B, the height of the barriers for the formate oxidation are lower than those computed for mechanism A (19.2 for triplet, and 23.1 kcal mol^{-1}, for singlet). In particular, the one computed as far as the high-spin is concerned is now in the range normally accepted for the enzymatic catalysis.

The formation of the EPb product is exothermic for both electronic states.

Computations in the protein environment also indicate the triplet PES as the minimum energy path, with an activation energy of 16.6 kcal mol^{-1}, lower than the corresponding one in the vacuum.

A simple explanation for the reliability of the mechanism B with respect to the mechanism A can be found in the different values of net charge (see Table S1 in the Supporting Information) exhibited by selenium in some key stationary points on the PESs. When the selenium atom is coordinated to the molybdenum atom (mechanism A), the lone pair necessary to abstract the proton from the substrate is not fully available because it is involved in the bonding with the cluster (the net charge on Se is 0.149 and 0.062 $|e|$, in the ESa singlet and triplet species, respectively).

In the case of mechanism B, the net charge on Se is -0.242 for singlet ESb and -0.319 $|e|$ for the triplet ESb. This different charge distribution accounts for the better character of catalytic base exhibited by the SeCys140 residue in the mechanism B.

Thus, we can conclude that the selenium atom is a better base at performing the proton abstraction from the substrate when it is not bound to the metallic centre because in this case, the lone pair present on the negative selenocysteine is more available.

The role played by the Arg333 residue is to stabilize the negative charge on the free selenol and to favour the coordination of the $HCOO^-$ to the metallic centre by orienting the latter into a good position to undergo oxidation. For the step sequence considered here, the His141 residue is involved in catalysis by establishing weak interactions with the active site.

The main role is played by the catalytic base SeCys140, so that the molybdenum has to first anchor the substrate in a good position to be oxidized, and later participate in the catalysis by accepting the electrons that come upon oxidation.

Although FDH and the other enzymes from the DMSO reductase family catalyze very different reactions, we note that, for the mechanism B, activation energies that occur in the FDH catalysis are not so different from those obtained for nitrate reductase ($\Delta E^{\pm} = 19.3$ kcal mol^{-1}).[33]

All these calculations were performed by assuming a small effect on the energetic profiles by the surrounding protein, which we have simulated by dielectric continuum methods in the framework of a static representation of the studied systems. In addition to these QM computations, other calculations regarding the surrounding protein and the dynamic behaviour should be carried out through QM/MM and MD methods to enlarge the knowledge of the working mechanism of this enzyme.

Prediction of barrier height of H-GGA and HM-GGA methods: Table 1 summarizes the gas-phase activation energies computed for mechanism B at different levels of theory. They were computed by considering the high-spin electronic state.

Table 1. Activation energy (in kcal mol^{-1}) for the formate oxidation by formate dehydrogenase at different DF levels.

	Activation energy [kcal mol^{-1}]
B3LYP	19.2
BHandHLYP	17.9
MPWB1K	23.6
BB1K	22.8
PBE1PBE	19.9

H-GGA BHandHLYP and PBE1PBE provide an activation energy of 17.9 and 19.9 kcal mol^{-1}, respectively. These values are very similar to the one obtained with B3LYP (19.2 kcal mol^{-1}); PBE1PBE is the one that more closely matches. This is quite expected because the behaviour of the B3LYP functional is closer to the one of PBE1PBE rather than to the BHandLYP, as was obtained for non-H-atom transfer and H-atom transfer barrier heights.[52]

The values obtained with the HM-GGA functionals are 23.6 kcal mol^{-1} for MPWB1K, and 22.8 kcal mol^{-1} for BB1K, with a difference of 0.8 kcal mol^{-1} between them. The similarity of these two methods in the barrier height determination is in agreement with the literature.[37]

H-GGA methods are found to provide smaller activation energies than the HM-GGA methods, which seem to overestimate the barrier heights. Taking into account the most recent benchmarking studies,[37] the B3LYP functional seems to provide lower activation energies for our investigation too.

To our knowledge, no kinetic data exist on Mo-containing formate dehydrogenase, so that a direct comparison cannot be made.

Conclusions

The catalytic mechanism of the Mo-containing formate dehydrogenase H enzyme was widely investigated at the density functional level of theory. The model cluster used to simulate the active site of the enzyme was large enough to reliably reproduce the oxidation of the formate molecule to CO_2 as it is performed by this enzyme in the hydrogen metabolic pathway.

The two different mechanisms derived from the presence of bound (mechanism A) or unbound (mechanism B) selenocysteine residue to the molybdenum site were taken into account. For both mechanisms, two different electronic states (singlet and triplet) were considered.

The oxidation reaction starts with the formation of a complex between the substrate and the active site by the coordination of formate oxygen atom to the metal. Next, abstrac-

tion of the proton from the formate carbon atom by the selenium atom of the SeCys140 residue leads finally to the products.

The activation barrier involved in the mechanism A, in which the SeCys140 residue is retained as the Mo ligand, was found to be higher than that computed for mechanism B; this indicates that the oxidation reaction of $HCOO^-$ is kinetically favoured when this residue is in the unbound form. Mechanism A is also unfavourable from the thermodynamic point of view. Activation barriers become suitable for catalysis only when the cluster is present as a high-spin triplet species.

The Arg333 residue, which is highly conserved among all the formate dehydrogenases H has a key role in catalysis because it stabilizes the negative charge present on the free selenol.

The effects of the solvent are quite small, and, in the case of minimum energetic path, reduce the activation barrier of 2.6 kcal mol^{-1}.

Gas-phase activation energies have been computed with some DFT functionals. HM-GGA methods, such as BB1K and MPWB1K, provide a value for the activation energy that is higher than the B3LYP one.

Based on these findings, the "unbound SeCys" mechanism can be regarded with confidence as the preferred reaction path followed by the Mo-containing formate dehydrogenase enzyme.

Acknowledgement

The University of Calabria and Regione Calabria (POR 2000/2006, misura 3.16, progetto PROSICA) are gratefully acknowledged.

[1] B. K. Burgess, D. J. Lowe, *Chem. Rev.* **1996**, *96*, 2983.
[2] R. Hille, *Chem. Rev.* **1996**, *96*, 2757.
[3] A. Thapper, C. Lorber, J. Fryxelius, A. Behrens, E. Nordlander, *J. Inorg. Biochem.* **2000**, *79*, 67.
[4] R. Hille, *J. Biol. Inorg. Chem.* **1996**, *1*, 397.
[5] D. Collison, C. D. Garner, J. A. Juole, *Chem. Soc. Rev.* **1996**, *25*, 25.
[6] B. L. Berg, J. Li, J. Heider, V. Stewart, *J. Biol. Chem.* **1991**, *266*, 22380.
[7] H. Abaibou, J. Pommier, G. Giordano, M. A. Mandrand-Berthelot, *J. Bacteriol.* **1995**, *177*, 7141.
[8] J. C. Boyington, V. N. Gladyshev, S. V. Khangulov, T. C. Stadtman, P. D. Sun, *Science* **1997**, *275*, 1305.
[9] H. C. A. Raaijmakers, M. J. Romao, *J. Biol. Inorg. Chem.* **2006**, *11*, 849.
[10] M. G. Rivas, P. J. Gonzalez, C. D. Brondino, J. J. G. Moura, I. Moura, *J. Inorg. Biochem.* **2007**. *101*, 1617.
[11] Gaussian 03, Revision C.02, M. J. Frisch, G. W. Trucks, H. B. Schlegel, G. E. Scuseria, M. A. Robb, J. R. Cheeseman, J. A. Montgomery, Jr., T. Vreven, K. N. Kudin, J. C. Burant, J. M. Millam, S. S. Iyengar, J. Tomasi, V. Barone, B. Mennucci, M. Cossi, G. Scalmani, N. Rega, G. A. Petersson, H. Nakatsuji, M. Hada, M. Ehara, K. Toyota, R. Fukuda, J. Hasegawa, M. Ishida, T. Nakajima, Y. Honda, O. Kitao, H. Nakai, M. Klene, X. Li, J. E. Knox, H. P. Hratchian, J. B. Cross, V. Bakken, C. Adamo, J. Jaramillo, R. Gomperts, R. E. Stratmann, O. Yazyev, A. J. Austin, R. Cammi, C. Pomelli, J. W. Ochterski, P. Y. Ayala, K. Morokuma, G. A. Voth, P. Salvador, J. J. Dannenberg, V. G. Zakrzewski, S. Dapprich, A. D. Daniels, M. C. Strain, O. Farkas, D. K. Malick, A. D. Rabuck, K. Raghavachari, J. B. Foresman, J. V. Ortiz, Q. Cui, A. G. Baboul, S. Clifford, J. Cioslowski, B. B. Stefanov, G. Liu, A. Liashenko, P. Piskorz, I. Komaromi, R. L. Martin, D. J. Fox, T. Keith, M. A. Al-Laham, C. Y. Peng, A. Nanayakkara, M. Challacombe, P. M. W. Gill, B. Johnson, W. Chen, M. W. Wong, C. Gonzalez, J. A. Pople, Gaussian, Inc., Pittsburgh PA, **2003**.
[12] A. D. Becke, *J. Chem. Phys.* **1993**, *98*, 5648–5652.
[13] C. Lee, W. Yang, R. G. Parr, *Phys. Rev. B* **1988**, *37*, 785–789.
[14] A. D. Becke, *J. Chem. Phys.* **1993**, *98*, 1372.
[15] A. D. Becke, *Phys. Rev. A* **1988**, *38*, 3098.
[16] R. Ditchfield, W. J. Hehre, J. A. Pople, *J. Chem. Phys.* **1971**, *54*, 724–728.
[17] W. J. Hehre, R. Ditchfield, J. A. Pople, *J. Chem. Phys.* **1972**, *56*, 2257–2261.
[18] P. C. Hariharan, J. A. Pople, *Mol. Phys.* **1974**, *27*, 209–214.
[19] M. S. Gordon, *Chem. Phys. Lett.* **1980**, *76*, 163–168.
[20] P. J. Hay, W. R. Wadt, *J. Chem. Phys.* **1985**, *82*, 270–283; P. J. Hay, W. R. Wadt, *J. Chem. Phys.* **1985**, *82*, 284–298; P. J. Hay, W. R. Wadt, *J. Chem. Phys.* **1985**, *82*, 299–310.
[21] C. Gonzalez, H. B. Schlegel, *J. Chem. Phys.* **1989**, *90*, 2154.
[22] C. Gonzalez, H. B. Schlegel, *J. Phys. Chem.* **1990**, *94*, 5523.
[23] R. Seeger, J. A. Pople, *J. Chem. Phys.* **1977**, *66*.
[24] R. Bauernschmitt, R. Ahlrichs, *J. Chem. Phys.* **1996**, *104*, 9047.
[25] H. B. Schlegel, J. J. McDouall in *Computational Advances in Organic Chemistry*, (Eds.: C. Ogretir, I. G. Csizmadia), Kluwer Academic, The Netherlands, **1991**, 167–185.
[26] S. Miertus, E. Scrocco, J. Tomasi, *Chem. Phys.* **1981**, *55*, 117–129.
[27] S. Miertus, J. Tomasi, *Chem. Phys.* **1982**, *65*, 239–245.
[28] M. Cossi, V. Barone, R. Commi, J. Tomasi, *Chem. Phys. Lett.* **1996**, *255*, 327.
[29] V. Barone, M. Cossi, B. Menucci, J. Tomasi, *J. Chem. Phys.* **1997**, *107*, 3210–3221.
[30] P. E. M. Siegbahn, M. R. A. Blomberg, *Chem. Rev.* **2000**, *100*, 421–437.
[31] L. Noodleman, T. Lovell, W. G. Han, J. Li, F. Himo, *Chem. Rev.* **2004**, *104*, 459–508.
[32] T. Marino, N. Russo, M. Toscano, *J. Am. Chem. Soc.* **2005**, *127*, 4242–4253.
[33] M. Leopoldini, N. Russo, M. Toscano, M. Dulak, A. T. Wesoloski, *Chem. Eur. J.* **2006**, *12*, 2532–2541.
[34] M. Leopoldini, N. Russo, M. Toscano, *J. Phys. Chem. A* **2006**, *110*, 1063–1072.
[35] M. Leopoldini, N. Russo, M. Toscano, *Chem. Eur. J.* **2007**, *13*, 2109–2117.
[36] M. Leopoldini, N. Russo, M. Toscano, *J. Am. Chem. Soc.* **2007**, *129*, 7776–7784.
[37] S. F. Sousa, P. A. Fernandes, M. J. Ramos, *J. Phys. Chem. A* **2007**, *111*, 10439–10452, and references therein.
[38] B. J. Lynch, D. G. Truhlar, *J. Phys. Chem. A* **2001**, *105*, 2936–2941.
[39] Y. Zhao, J. Pu, B. J. Lynch, D. G. Truhlar, *Phys. Chem. Chem. Phys.* **2004**, *6*, 673–676.
[40] D. K. Malick, G. A. Peterson, J. A. Montomery, Jr., *J. Chem. Phys.* **1998**, *108*, 5704–5713.
[41] K. T. Kuwata, K. L. Templeton, A. S. Hasson, *J. Phys. Chem. A* **2003**, *107*, 11525–11532.
[42] M. L. Coote, *J. Phys. Chem. A* **2004**, *108*, 3865–3872.
[43] Y. Zhao, B. J. Lynch, D. G. Truhlar, *J. Phys. Chem. A* **2004**, *108*, 2715–2719.
[44] Y. Zhao, D. G. Truhlar, *J. Phys. Chem. A* **2004**, *108*, 6908–6918.
[45] J. P. Perdew, K. Burke, M. Ernzerhof, *Phys. Rev. Lett.* **1996**, *77*, 3865–3868.
[46] A. D. Becke, *J. Chem. Phys.* **1996**, *104*, 1040–1046.
[47] C. Adamo, V. Barone, *J. Chem. Phys.* **1998**, *108*, 664–675.
[48] E. D. Glendening, A. E. Reed, J. E. Carpenter, F. Weinhold, *NBO*, Version 3.1.
[49] C. A. McDevitt, G. R. Hanson, C. J. Noble, M. R. Cheesman, A. G. McEwan, *Biochemistry* **2002**, *41*, 15234–15244.

[50] T. Waters; X-B. Wang, X. Yang, L. Zhang, R. A. J. O'Hair, L.-S. Wang, A. G. Wedd, *J. Am. Chem. Soc.* **2004**, *126*, 5119–5129; X-B. Wang, X. Yang, L. Zhang, R. A. J. O'Hair, L.-S. Wang, A. G. Wedd, *J. Am. Chem. Soc.* **2004**, *126*, 5119–5129.

[51] M. Kaupp, *Angew. Chem.* **2004**, *116*, 554–558; *Angew. Chem. Int. Ed.* **2004**, *43*, 546–549.

[52] Y. Zhao, N. Gonzales-Garcia, D. G. Thrular, *J. Phys. Chem. A* **2005**, *109*, 2012–2018.

Received: May 12, 2008
Published online: August 1, 2008

